

Investigate on structure for transparent anti-icing surfaces F

Cite as: AIP Advances 10, 085101 (2020); <https://doi.org/10.1063/5.0019119>

Submitted: 23 June 2020 . Accepted: 07 July 2020 . Published Online: 04 August 2020

Nguyen Ba Duc , and Nguyen Thanh Binh

COLLECTIONS

F This paper was selected as Featured



View Online



Export Citation




CrossMark



NEW!

Sign up for topic alerts
New articles delivered to your inbox



Investigate on structure for transparent anti-icing surfaces

Cite as: AIP Advances 10, 085101 (2020); doi: 10.1063/5.0019119

Submitted: 23 June 2020 • Accepted: 7 July 2020 •

Published Online: 4 August 2020



View Online



Export Citation



CrossMark

Nguyen Ba Duc^{1,a)}  and Nguyen Thanh Binh^{2,b)}

AFFILIATIONS

¹Faculty of Physics, Tan Trao University, Tuyen Quang Province, 30000, Vietnam

²Faculty of Physics, Thai Nguyen University of Education, Thai Nguyen Province, 21000, Vietnam

^{a)}ducnb@daihoctantrao.edu.vn

^{b)}Author to whom correspondence should be addressed: nguyenthanhbinh.dhsptn@gmail.com

ABSTRACT

The ice-phobic and transparent surface based on the distinctive structure of a coating material has been investigated. Moth eye structure fabricated on the quartz substrate was covered with a flat paraffin layer to isolate it in a cold and humid environment. Paraffin wax was chosen as the coating material due to low thermal conductivity, easy coating, and original water repellency. The paraffin layer only stayed on the top of the nanostructure, separated it from the outside environment to obstruct heat energy being transferred to the cold substrate, and prevented the wetting transition, which was observed regularly on the rough surface. The uncountable number of air blocks trapped inside the nanostructure also contributed to delayed heat transfer, leading to an increase in the freezing time of the attached water droplet. The anti-icing performance was evaluated in terms of adhesion strength, freezing time, and freezing rain sustainability. The nanostructure coated sample was compared with barely coated and superhydrophobic nanostructure surface and demonstrated a preeminent performance.

© 2020 Author(s). All article content, except where otherwise noted, is licensed under a Creative Commons Attribution (CC BY) license (<http://creativecommons.org/licenses/by/4.0/>). <https://doi.org/10.1063/5.0019119>

I. INTRODUCTION

Ice accumulation on aircraft wings can reduce lifting force, block moving parts, and cause disastrous problems.^{1,2} Ice accretion on energy transmission systems,³ vehicles, and ships in a harsh environment often leads to massive destruction and contributes to serious accidents.

Many studies have been conducted over several decades to improve the anti-icing performance on functional surfaces and, in general, the improvement measures are often divided into active and passive approaches. While active approaches correspond to the ice removal via an external energy source,^{4–6} passive approaches refer to physicochemical methods^{7–9} based on the surface modification. Among many reported passive approaches, the superhydrophobic surface (SHS) was believed to be the appropriate solution for anti-icing owing to its unique characteristics of water repellency (high contact angle and low sliding angle) and facile fabrication.^{10–18} However, several studies have recently revealed that SHS may not always be the optimal approach for anti-icing due to its sensitivity to

humidity, especially under low-temperature conditions,^{19–23} leading to the wetting transition from Cassi–Baxter to Wenzel state. Therefore, the ice formed easily adheres to the surface of the material, reduces the hydrophobic coating, and is harder to clean than smooth surfaces.

Recently, biomimetic slippery liquid infused porous surfaces (SLIPs) have been introduced as an advanced anti-icing strategy.^{24–27} This new concept presents a defect-free liquid interface with the relevant properties such as water immiscibility, humidity tolerance, and self-healing after ice removal.^{8,28–37} SLIPs can be fabricated through covering a porous structure with a low-surface-tension lubricant that is immiscible in water and has a high affinity with structured materials. Even though SLIPs has improved anti-icing efficiency, it is impossible to permanently prevent the icing phenomenon owing to the degradation of the lubricant layer through evaporation and during the removal process.

In this work, the anti-icing properties of the unique nanostructure coated paraffin surfaces were evaluated in terms of adhesion strength, freezing time, and mimicking rain sustainability. Results

were compared with bare quartz coated paraffin, superhydrophobic nanostructure surfaces, and demonstrated the outstanding anti-icing performance. The contribution of the paraffin layer and air block combined with the nanostructure was explained as the important criteria for maintaining stable adhesion strength and extending freezing time. Furthermore, the nanostructure coated sample also exhibits high transparency and anti-reflective effects owing to the moth eye structure,³⁸ indicating the potential designs for practical optical applications.

II. EXPERIMENTAL SECTION

A. Sample fabrication

The experiments were performed with a quartz glass substrate due to its facile fabrication. The details of the fabrication process are described in Fig. 1. Quartz substrates were first cleaned with detergent (Alconox, Sigma-Aldrich, Inc.), deionized water, followed by drying with N₂ gas flow. After ultraviolet-ozone treatment, the surface was coated with a monolayer of polystyrene (PS) beads (Polyscience, Inc.) of diameter 200 nm via the floating method.

The nanostructure was imposed on the substrate by the plasma etching process. A gas mixture of O₂, CF₄, and H₂ with appropriate concentration and ratio was bombarded onto the substrate. By

manipulating the size reduction process and etching time, we can generate a uniform truncated cone shape with a height of 500 nm and a top diameter around 70 nm. Etched surfaces were immersed in the as-prepared 0.1% perfluoropolyether (PFPE, Soilnon AF30, Niccakorea Co., Ltd.) solution for 1 h, followed by drying under ambient conditions for 1 h.

The coating procedure was conducted using the spin coating method. Paraffin wax (0.5g) was added to 10 ml of n-hexane for preparing a coating solution. After stirring for 30 min, the suspension was deposited on a superhydrophobic nanostructure surface using a spin coater (5000 rpm, 2 min, accelerated speed 500 rpm/10 s). The same process was carried out on bare quartz under relevant conditions to create the same thickness of the paraffin layer. After coating, samples were dried naturally at room temperature for 1 h.

B. Characterization of prepared surfaces

Surface morphologies were examined using a scanning electron microscope (SEM, Quanta 250, FEI). Etched samples presented a uniform truncated cone shape nanopillar array on a quartz substrate with a height of around 500 nm. After spin coating process, a thin layer of paraffin was deposited on top of the nanostructure, which isolated it from the outside environment [Fig. 1(b)].

The wettability of the prepared samples was obtained by measuring the contact angles (CA) and sliding angles (SA) using a contact angle measurement apparatus (Model DM-50, Kyowa Interface Science Co., Ltd.). All values were averaged statistically for at least five independent positions on each sample (Fig. 2). The wetting characteristics are summarized in Table I.

The transparency and anti-reflective properties of the prepared surfaces were characterized using an optical measurement apparatus (Angle Resolving Spectrometer, Agilent Technologies). Results were compared by using the bare surface as a reference.

C. Setup for anti-icing measurements

The measurement of adhesion force was performed using a custom-built apparatus, as shown in Fig. 3. The prepared samples were attached to the thermoelectric cooling module using Al tape. A 5 μ l deionized water droplet was gently placed on the sample surface, and then, the system was cooled until the temperature reached -20°C . After the phase transition, a load cell was used to measure the adhesion strength between the ice drop and the cold surface. The load cell was controlled by a motorized linear stage, moving at a speed of 50 $\mu\text{m/s}$, and slowly pushed the ice droplet horizontally until it detached completely. The load cell probe was kept at 0.5 mm above the surface to minimize torque. The force exerted on the load cell can be obtained through computer software, and the maximum force recorded was considered as the adhesive strength.

A high-speed camera (Photron, Ltd.) was used to record the icing process and determine the freezing time. Freezing time is defined as the duration from the time the water droplet started changing from the liquid phase to the solid phase until the whole droplet became ice. Another camera was used to capture the temperature change of the water droplet–solid interface.

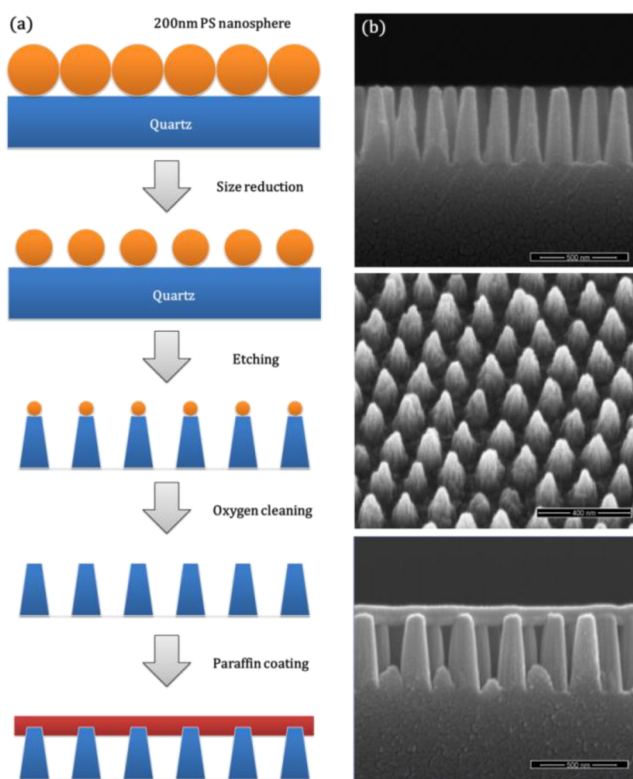


FIG. 1. (a) Fabrication process and (b) SEM images.

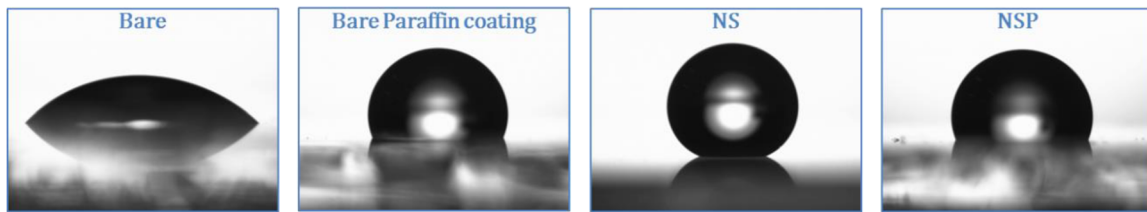


FIG. 2. Contact angle on prepared surfaces.

III. RESULTS AND DISCUSSIONS

A. Anti-icing performance

The samples were treated under different conditions to determine the individual effect of the nanostructure, hydrophobicity, and paraffin layer. Figure 4 presents the adhesion strength measurements on three prepared samples: barely coated paraffin, nanostructure superhydrophobic (NS), and superhydrophobic nanostructure coated paraffin (NSP) surfaces. The lowest adhesive strength is for the NS sample, followed by the NS coated paraffin, while the barely coated sample exhibits quite high value due to the good affinity between quartz and paraffin. The low adhesion strength on the NS sample can be explained by the areal fraction between the ice droplet and textured surface.³⁸ The water droplet was kept at the Cassie-Baxter state in the whole freezing process, resulting in the

low contact area between the ice droplet and the textured structure. The lower the areal contact area we can support, the lower adhesion strength we have. However, the durability in anti-icing is very important due to the practical applications. A good performance of the anti-icing surfaces should be maintained for a long time, while hydrophobic coatings are not durable when exposed to cold and humid environments. As shown in Fig. 4, adhesion strength increases dramatically from around 30 kPa–370 kPa after 30 cycles (same as paraffin coated samples) and finally reached 1200 kPa after 100 cycles. The degradation shown in Fig. 4 can explain it. The adhesion strength of hydrophobic layer on prepared samples owes directly to the contacted frosting during the freezing process. A tiny droplet accumulated on the whole surface area even though inside the nanostructure is rapidly transferred to the solid phase and anchored to the structure. This may gradually damage the coating layer when we remove the ice sheets using mechanical force or airflow, subsequently leading to the vanishing of hydrophobicity.

In contrast to the NS surface, the water droplet on the NSP surface did not directly come in contact with the nanostructure but with the paraffin layer. Due to the large contact area with a smooth surface, the adhesion strength is quite high compared to the NS surface, but it shows very stable adhesion strength owing to the original properties of paraffin. The adhesion strength can be obtained around

TABLE I. Wetting characteristics of the prepared surfaces.

Sample	Contact angle (deg)	Sliding angle (deg)
Bare quartz	50	...
Bare paraffin coating	111	14
NS	155	2
NSP	114	8

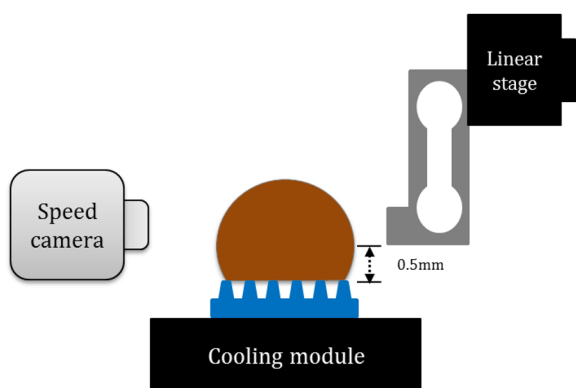


FIG. 3. Adhesion measurement setup.

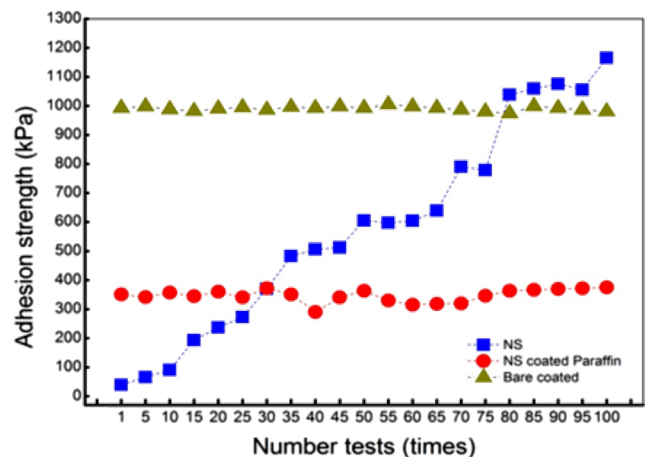


FIG. 4. Adhesion strength on prepared samples.

350 kPa and maintained after 100 cycles, showing the durability of the NSP surface in anti-icing. Interestingly, we cannot see any wetting transition due to the indirect contact between ice droplets and nanostructure. The waterdrop is maintained in the hydrophobic state ($CA \sim 115^\circ$) during the whole process due to the original water repellency of paraffin. The nanostructure was covered underneath and played its function in delaying heat transfer or anti-reflective effects. For the practical applications, NSP surfaces are considered as the advantageous solution compared to the NS sample owing to their durability after experimenting many times.

When adhesion strength on the NSP surface and on the barely coated surface is compared, the contribution of the nanostructure on reducing the adhesion strength is observed. It can be explained by the quite thin layer of paraffin that the NSP surface still exhibited the roughness compared to the smooth surface, which reduced the contact area and adhesion strength.

Furthermore, the temperature evolution in Table II revealed the big difference in heat delaying between the three prepared samples. We believe that the difference in the surface actual temperature played a crucial role in determining the adhesive force. In the barely coated surface, the icing process happened at -10.9°C as shown in the Peltier controller indicator, corresponding to 8.9°C difference between it and the surface–water contact interface temperature, while the difference in the NS and NSP samples is 9 and 11.4°C , corresponding to the actual temperature of -5.1°C and -1.7°C , respectively. This temperature delay can be explained by surface characterization. The combination of air traps and paraffin layers on the NSP surface was suitable to prevent the heat transfer from Peltier through the surface structure, leading to higher freezing temperatures and a longer time for the icing process. After cooling has started, the surface temperature of the barely coated sample needed 240 s to reach to -2°C , while the NSP sample required over 300 s to reach a comparable value (-1.7°C).

It is worth noting that frosting on the surface always occurred and balanced with the evaporation due to the surrounding environment fluctuation. However, the quite high rate of temperature decrease on a barely coated sample would lead to the fast accumulation of frosting droplets all over the surface, including the contact line of the three phases. These new nucleation droplets rapidly coalesced with water droplets and would increase the contact area. It can be seen in Fig. 5 that the increase in the contact area by 10%, from 1.93 mm to 2.13 mm, leads to a relatively high adhesion strength. In contrast, the low rate of the temperature decrease

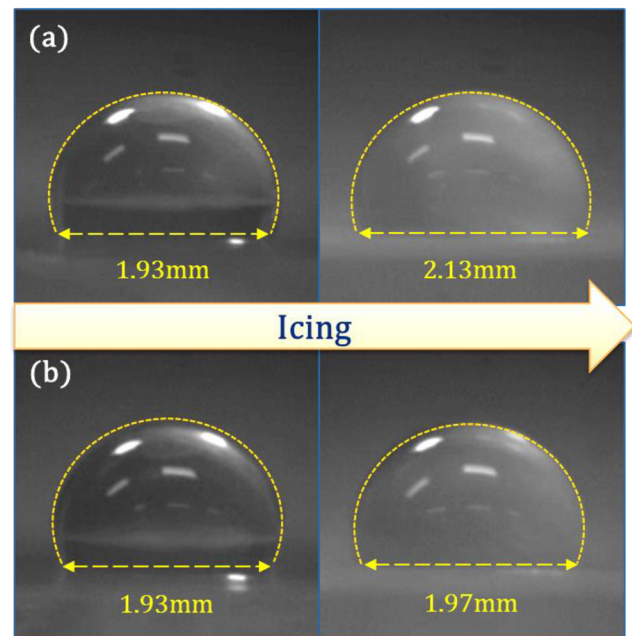


FIG. 5. Icing process on (a) barely coated sample and (b) NSP sample.

exhibited on the NSP surface resulted in the low frosting accumulation effects, therefore, maintaining the contact area until complete freezing.

Figure 6 presents the freezing time measurements on prepared samples under different conditions. The shortest freezing time can be observed on a barely coated surface with values around 17 s. Even though paraffin proposes bad thermal conductivity, it cannot support the long freezing time for water droplets due to a large contact area and a very thin coating layer. However, when we combined this

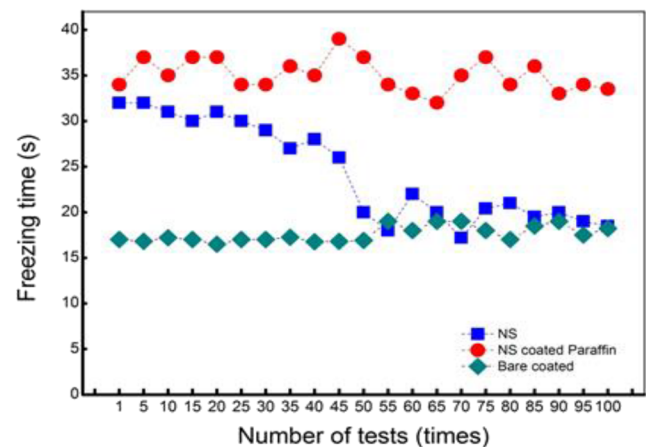


FIG. 6. Freezing time measurements on prepared samples.

TABLE II. Temperature and time for freezing.

Sample	Temperature at freezing point ($^\circ$)		Time (s)
	Top	Bottom	
Bare paraffin coating	-2	-10.9	240
NS	-5.1	-14.1	360
NSP	-1.7	-13.1	310

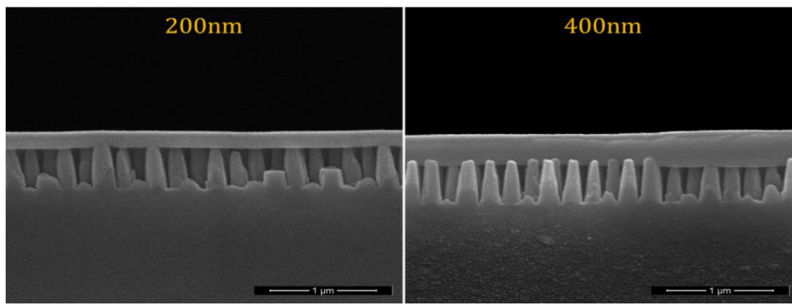


FIG. 7. Paraffin layer with different thicknesses.

thin paraffin layer with the nanostructure, as shown in NSP samples, it can dramatically increase the freezing time up to around 37 s. Its unique structure along with the thermal characteristics of paraffin can explain it. In this manner, the paraffin layer isolated water droplets from the surface, which has better thermal conductivity ($k = 1.3 \text{ W/m K}$).

In contrast to NS samples, the heat energy from the water droplet was transferred to the outermost layer instead of directly conducting to nanopillars. The paraffin layer played the role of a thermal insulator to delay heat flow, minimizing heat transfer per unit time to extend the freezing time. Besides, after passing through the paraffin layer, heat energy was dispersed to two separated parts: quartz nanopillars and air volumes before being transferred to the cold substrate. It is worth noting that numerous air blocks can play an important role in minimizing heat dispersion owing to very bad thermal conductivity.

The contribution of the paraffin layer can be seen clearly when comparing NSP with the NS sample. In the first experiments, NS showed good performance in delaying the freezing process, but after several cycles, the performance became worse due to the degradation of the hydrophobic coating. Water droplets can easily penetrate inside the nanostructure, resulting in the wetting transition to the Wenzel state, maximizing the contact area, therefore, shortening the freezing time. After 50 cycles, NS samples exhibit a short freezing

time of around 18 s, which is comparable to the bare coated surface while the NSP sample still maintained its properties even after experimenting 100 times.

The contribution of the thickness in anti-icing and transparent performance also has been evaluated. The concentration of paraffin in solution was varied with 2% and 3% to generate a thicker paraffin layer on the nanostructure (Fig. 7). Figure 8 describes the adhesion strength and freezing time with different thicknesses of paraffin. By increasing the thickness, the adhesive strength increased dramatically from 350 kPa in the original coating sample to 900 kPa (200 nm) and 970 kPa (400 nm), relatively close to the barely coated sample. The freezing time also decreased significantly from around 35 s to 20 s, indicating the nanostructure's negligible contribution.

For the freezing rain test, we sprayed cold water droplets with the random size ranging from $5 \mu\text{l}$ to $50 \mu\text{l}$ onto prepared surfaces in 5 min. Deionized water was kept at a temperature of around 0.5°C before flushing to surfaces to mimic the rain in cold environments. The temperature of substrates was maintained at 0°C , -5°C , -10°C , and -15°C for evaluating the temperature contribution. The performance of three functional surfaces can be obtained using a speed camera in the whole spraying process (Fig. 9). On a bare coated surface, due to the high contact area and the small difference in temperature between the outmost layer and the cold substrate, the

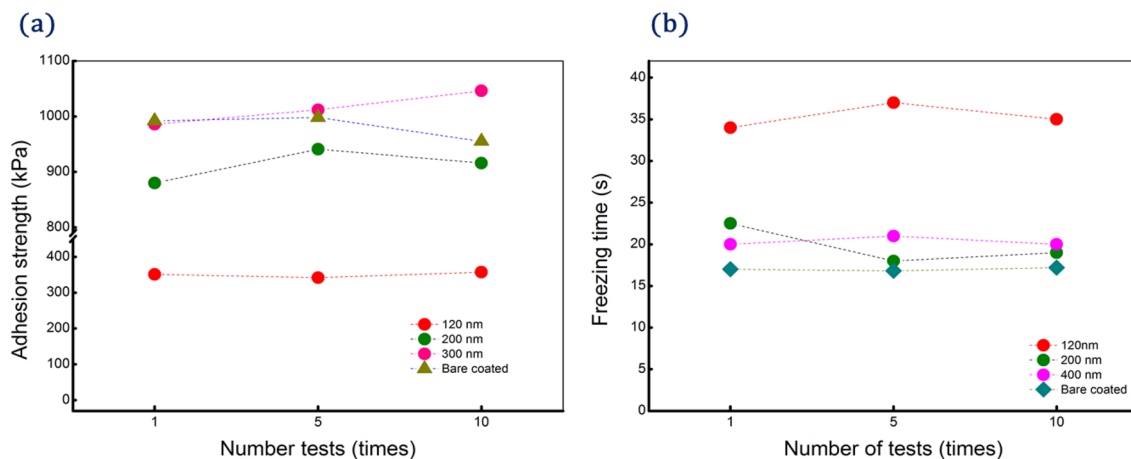


FIG. 8. (a) Adhesion strength and (b) freezing time with different thicknesses.

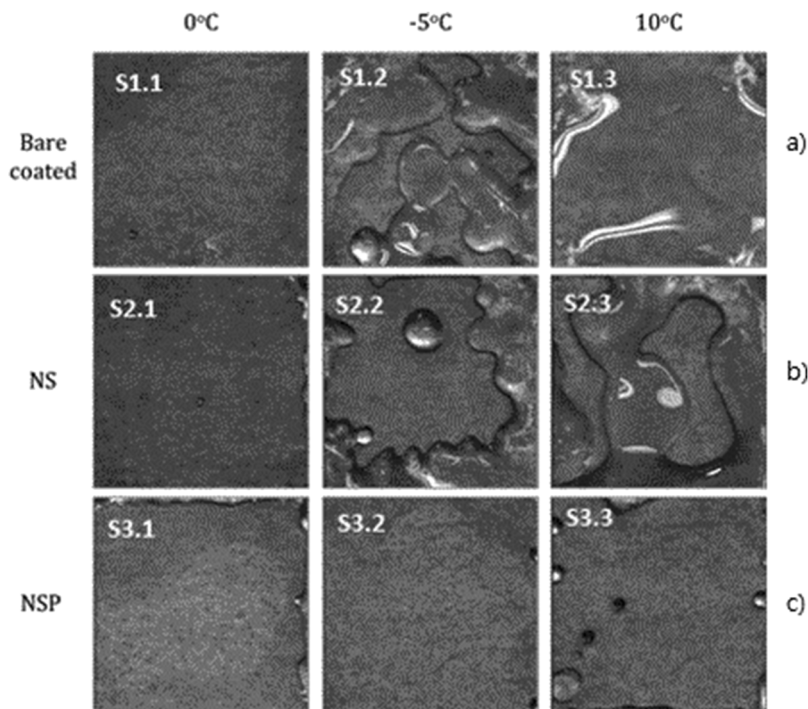


FIG. 9. Ice accumulation on (a) barely coated, (b) NS, and (c) NSP samples after the freezing test.

incoming water droplets may rapidly transfer their heat to the surface and freeze easily. As shown in the -5°C test (S1.2 of Fig. 9), after 45 s, ice droplets appeared and strongly adhered to the cold surface. Further water spraying tends to stick on the formed ice to increase the area until the surface is fully covered.

Due to the high hydrophobicity on the NS sample, water can easily bounce out from the surface and remain as a clear area at 0°C (S2.1 of Fig. 9). When temperature decreased to -5°C , a significant change in the anti-icing behavior was observed. Water droplets rapidly transferred its heat to the substrate and became ice drops.

Much ice nucleation can be seen on the surface after a short time spraying (S2.2 of Fig. 9). The performance became worst when the temperature was continuously decreased to -10°C when the ice layer almost covered the surface area after flushing water for 5 min (S2.3 of Fig. 9). In contrast, on the NSP sample, the clear surface was maintained even though when we decreased the temperature to -10°C , owing to the heat delaying effect (S3.3 of Fig. 9). Due to original water repellency of the paraffin film and indirect contact between the water droplets and the nanostructure, the temperature of the outermost layer was kept at a higher value than the NS

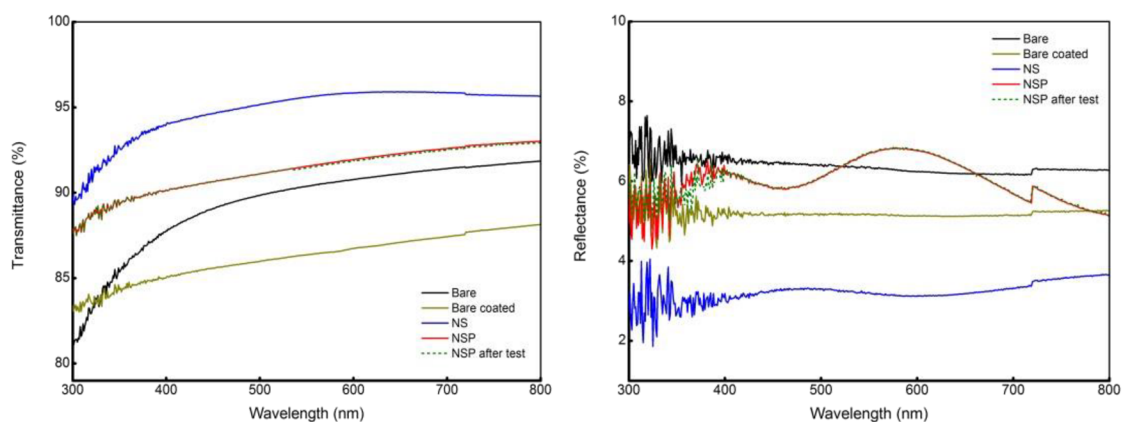


FIG. 10. Transmittance and reflectance spectra on prepared surfaces.



FIG. 11. Images of (a) original NSP sample, (b) after scratching, and (c) after healing.

sample, therefore, minimizing the ice nucleation process. The NSP sample still showed the anti-icing performance at a lower temperature (-15°C) when ice droplets appeared sparsely on the spraying area (S3.4 of Fig. 9).

B. Optical performance

The optical characteristics of the prepared samples were obtained by measuring the transmittance and reflectance performance using our spectrometer equipment. Figure 10(a) depicts the transmittance in a visible range of barely coated paraffin, NS, and NSP surfaces with barren quartz as the reference. Owing to the moth eye structure, NS enhances the transmittance compared to smooth surfaces. After coating with the paraffin layer, its transmittance negligibly decreases to $\sim 92\%$ but still higher than bare quartz. The competition between the optical advantage supported by moth eye structure and the disadvantage from the reflectance of the paraffin film is worth noting. However, the NSP sample still exhibits good transmittance and anti-reflective efficiency due to the very thin paraffin layer.

For practical applications, the durability of the NSP surface was also tested using a simple mechanical method (Fig. 11). The NSP surface was scratched using a sharp knife's tip to remove the paraffin cover layer. After scratching, the sample was heated at 80°C for 15 min and the transmittance was measured again. The dashed line and dotted line describe the performance before and after heating, respectively, revealing the full recovery of the optical performance. The melting of the paraffin layer can explain it after heating, and the easily covered surface resulted to be a smooth surface, maintaining its transmittance.

IV. CONCLUSION

In conclusion, we have investigated the transparency and anti-icing of various surfaces under different treatment conditions. Moth eye nanostructure paraffin coated surface exhibited greatly improved anti-icing performance, indicating the advantage of combining original water repellency and a unique heat-delaying structure. The hydrophobicity of the paraffin layer was specified as a decisive parameter for maintaining the adhesion strength between

ice and surface. For extending the freezing time on the functional surface, heat transfer from accumulated droplets should be interrupted when passing through the surface structure. Paraffin with quite low thermal conductivity worked as the thermal insulator to delay heat diffusion, therefore interfering with the icing process in both static (water droplet) and dynamic water (freezing rain) experiments.

We also determined that the NSP sample is also suitable for optical applications due to high transparency and anti-reflective properties. Owing to the minimal thickness, NSP exhibited good optical performance while maintaining its preeminence in ice-prevented work. Furthermore, the NSP sample also presented good mechanical sustainability. After mechanical tests, the paraffin coated layer was recovered easily by a simple heating method and exhibited stable anti-icing optical properties. This study is useful for understanding the importance of hydrophobicity and heat diffusion in designing anti-icing surfaces.

ACKNOWLEDGMENTS

This research was funded by the Vietnam National Foundation for Science and Technology Development (NAFOSTED) under Grant No. 103.02-2019.333.

The authors declare that they have no conflicts of interest.

DATA AVAILABILITY

The data that support the findings of this study are available from the corresponding author upon reasonable request.

REFERENCES

1. P. Tran, M. T. Brahim, I. Paraschivoiu, A. Pueyo, and F. Tezok, "Ice accretion on aircraft wings with thermodynamic effects," *J. Aircr.* **32**(2), 444–446 (1995).
2. J. Marwitz, M. Politovich, B. Bernstein, F. Ralph, P. Neiman, R. Ashenden, and J. Bresch, "Meteorological conditions associated with the ATR72 aircraft accident near Roselawn, Indiana, on 31 October 1994," *Bull. Am. Meteorol. Soc.* **78**(1), 41–52 (1997).
3. J. L. Laforte, M. A. Allaire, and J. Laflamme, "State-of-the-art on power line de-icing," *Atmos. Res.* **46**(1), 143–158 (1998).

- ⁴C. A. Martin and J. C. Putt, "Advanced pneumatic impulse ice protection system (PIIP) for aircraft," *J. Aircr.* **29**(4), 714–716 (1992).
- ⁵J. Palacios, E. Smith, J. Rose, and R. Royer, "Ultrasonic de-icing of wind-tunnel impact icing," *J. Aircr.* **48**(3), 1020–1027 (2011).
- ⁶L. Makkonen, T. Laakso, M. Marjaniemi, and K. J. Finstad, "Modelling and prevention of ice accretion on wind turbines," *Wind Eng.* **25**(1), 3–21 (2001).
- ⁷H. Cho, J. Lee, S. Lee, and W. Hwang, "Durable superhydrophilic/phobic surfaces based on green patina with corrosion resistance," *Phys. Chem. Chem. Phys.* **17**(10), 6786–6793 (2015).
- ⁸G. Zhang, J. Hu, Y. Tu, G. He, F. Li, H. Zou, S. Lin, and G. Yang, "Preparation of superhydrophobic films based on the diblock copolymer P(TFEMA-*r*-Sty)-*b*-PCMA," *Phys. Chem. Chem. Phys.* **17**(29), 19457–19464 (2015).
- ⁹J. B. Boreyko, B. R. Srijanto, T. D. Nguyen, C. Vega, M. Fuentes-Cabrera, and C. P. Collier, "Dynamic defrosting on nanostructured superhydrophobic surfaces," *Langmuir* **29**(30), 9516–9524 (2013).
- ¹⁰J. Yang and W. Li, "Preparation of superhydrophobic surfaces on Al substrates and the anti-icing behavior," *J. Alloys Compd.* **576**, 215–219 (2013).
- ¹¹K. Li, X. Zeng, H. Li, and X. Lai, "A study on the fabrication of superhydrophobic iron surfaces by chemical etching and galvanic replacement methods and their anti-icing properties," *Appl. Surf. Sci.* **346**, 458–463 (2015).
- ¹²Z. Zuo, R. Liao, C. Guo, Y. Yuan, X. Zhao, A. Zhuang, and Y. Zhang, "Fabrication and anti-icing property of coral-like superhydrophobic aluminum surface," *Appl. Surf. Sci.* **331**, 132–139 (2015).
- ¹³S. A. Kulinich and M. Farzaneh, "Ice adhesion on super-hydrophobic surfaces," *Appl. Surf. Sci.* **255**(18), 8153–8157 (2009).
- ¹⁴D. K. Sarkar and M. Farzaneh, "Superhydrophobic coatings with reduced ice adhesion," *J. Adhes. Sci. Technol.* **23**(9), 1215–1237 (2009).
- ¹⁵S. Farhadi, M. Farzaneh, and S. A. Kulinich, "Anti-icing performance of superhydrophobic surfaces," *Appl. Surf. Sci.* **257**(14), 6264–6269 (2011).
- ¹⁶A. J. Meuler, J. D. Smith, K. K. Varanasi, J. M. Mabry, G. H. McKinley, and R. E. Cohen, "Relationships between water wettability and ice adhesion," *ACS Appl. Mater. Interfaces* **2**(11), 3100–3110 (2010).
- ¹⁷Y. Zhang, X. Yu, H. Wu, and J. Wu, "Facile fabrication of superhydrophobic nanostructures on aluminum foils with controlled-condensation and delayed-icing effects," *Appl. Surf. Sci.* **258**(20), 8253–8257 (2012).
- ¹⁸Q. Liu, Y. Yang, M. Huang, Y. Zhou, Y. Liu, and X. Liang, "Durability of a lubricant-infused electrospray silicon rubber surface as an anti-icing coating," *Appl. Surf. Sci.* **346**, 68–76 (2015).
- ¹⁹J. Chen, J. Liu, M. He, K. Li, D. Cui, Q. Zhang, X. Zeng, Y. Zhang, J. Wang, and Y. Song, "Superhydrophobic surfaces cannot reduce ice adhesion," *Appl. Phys. Lett.* **101**(11), 111603 (2012).
- ²⁰K. K. Varanasi, T. Deng, J. D. Smith, M. Hsu, and N. Bhate, "Frost formation and ice adhesion on superhydrophobic surfaces," *Appl. Phys. Lett.* **97**(23), 234102 (2010).
- ²¹K. Rykaczewski, S. Anand, S. B. Subramanyam, and K. K. Varanasi, "Mechanism of frost formation on lubricant-impregnated surfaces," *Langmuir* **29**(17), 5230–5238 (2013).
- ²²S. Bengaluru Subramanyam, V. Kondrashov, J. Rühle, and K. K. Varanasi, "Low ice adhesion on nano-textured superhydrophobic surfaces under supersaturated conditions," *ACS Appl. Mater. Interfaces* **8**(20), 12583–12587 (2016).
- ²³S. Jung, M. Dorrestijn, D. Raps, A. Das, C. M. Megaridis, and D. Poulikakos, "Are superhydrophobic surfaces best for icephobicity?," *Langmuir* **27**(6), 3059–3066 (2011).
- ²⁴T.-S. Wong, S. H. Kang, S. K. Y. Tang, E. J. Smythe, B. D. Hatton, A. Grinthal, and J. Aizenberg, "Bioinspired self-repairing slippery surfaces with pressure-stable omniphobicity," *Nature* **477**(7365), 443–447 (2011).
- ²⁵X. Yao, Y. Hu, A. Grinthal, T.-S. Wong, L. Mahadevan, and J. Aizenberg, "Adaptive fluid-infused porous films with tunable transparency and wettability," *Nat. Mater.* **12**(6), 529–534 (2013).
- ²⁶N. Vogel, R. A. Belisle, B. Hatton, T.-S. Wong, and J. Aizenberg, "Transparency and damage tolerance of patternable omniphobic lubricated surfaces based on inverse colloidal monolayers," *Nat. Commun.* **4**, 2176 (2013).
- ²⁷P. W. Wilson, W. Lu, H. Xu, P. Kim, M. J. Kreder, J. Alvarenga, and J. Aizenberg, "Inhibition of ice nucleation by slippery liquid-infused porous surfaces (SLIPS)," *Phys. Chem. Chem. Phys.* **15**(2), 581–585 (2013).
- ²⁸R. Dou, J. Chen, Y. Zhang, X. Wang, D. Cui, Y. Song, L. Jiang, and J. Wang, "Anti-icing coating with an aqueous lubricating layer," *ACS Appl. Mater. Interfaces* **6**(10), 6998–7003 (2014).
- ²⁹P. Kim, T.-S. Wong, J. Alvarenga, M. J. Kreder, W. E. Adorno-Martinez, and J. Aizenberg, "Liquid-infused nanostructured surfaces with extreme anti-ice and anti-frost performance," *ACS Nano* **6**(8), 6569–6577 (2012).
- ³⁰S. B. Subramanyam, K. Rykaczewski, and K. K. Varanasi, "Ice adhesion on lubricant-impregnated textured surfaces," *Langmuir* **29**(44), 13414–13418 (2013).
- ³¹J. Chen, R. Dou, D. Cui, Q. Zhang, Y. Zhang, F. Xu, X. Zhou, J. Wang, Y. Song, and L. Jiang, "Robust prototypical anti-icing coatings with a self-lubricating liquid water layer between ice and substrate," *ACS Appl. Mater. Interfaces* **5**(10), 4026–4030 (2013).
- ³²S. Ozbay, C. Yuceel, and H. Y. Erbil, "Improved icephobic properties on surfaces with a hydrophilic lubricating liquid," *ACS Appl. Mater. Interfaces* **7**(39), 22067–22077 (2015).
- ³³Y. H. Yeong, C. Wang, K. J. Wynne, and M. C. Gupta, "Oil-infused superhydrophobic silicone material for low ice adhesion with long-term infusion stability," *ACS Appl. Mater. Interfaces* **8**(46), 32050–32059 (2016).
- ³⁴L. Zhu, J. Xue, Y. Wang, Q. Chen, J. Ding, and Q. Wang, "Ice-phobic coatings based on silicon-oil-infused polydimethylsiloxane," *ACS Appl. Mater. Interfaces* **5**(10), 4053–4062 (2013).
- ³⁵T. Wang, Y. Zheng, A.-R. O. Raji, Y. Li, W. K. A. Sikkema, and J. M. Tour, "Passive anti-icing and active deicing films," *ACS Appl. Mater. Interfaces* **8**(22), 14169–14173 (2016).
- ³⁶C. Stamatopoulos, J. Hemrle, D. Wang, and D. Poulikakos, "Exceptional anti-icing performance of self-impregnating slippery surfaces," *ACS Appl. Mater. Interfaces* **9**(11), 10233–10242 (2017).
- ³⁷P. Juuti, J. Haapanen, C. Stenroos, H. Niemelä-Anttonen, J. Harra, H. Koivuloto, H. Teisala, J. Lahti, M. Tuominen, J. Kuusipalo *et al.*, "Achieving a slippery, liquid-infused porous surface with anti-icing properties by direct deposition of flame synthesized aerosol nanoparticles on a thermally fragile substrate," *Appl. Phys. Lett.* **110**(16), 161603 (2017).
- ³⁸S. Ji, K. Song, T. B. Nguyen, N. Kim, and H. Lim, "Optimal moth eye nanostructure array on transparent glass towards broadband antireflection," *ACS Appl. Mater. Interfaces* **5**(21), 10731–10737 (2013).